# Advanced Oxidation Processes (AOP) for Methylene Blue Degradation Using $ZnO_{75}\%$-$CdO_{25}\%$ Composite Nanocatalysts

**Vikas G. Patil[1], Dhananjay V. Mane[2], Sunanda V. Patil[3]**

[1]Research Scholor, School of Sciences, YCMOU Nashik 420003 India & Department of Sciences, K. J. Somaiya Polytechnic Mumbai 400077 India
[2]Former. Regional Director, YCMOU Nashik 420003 India & Department of Chemistry, Shri Chhatrapati Shivaji College Omerga, Dharashiv 413606 India

**Abstract**
This study examines the photocatalytic degradation of Methylene Blue (MB) using zinc oxide-cadmium oxide ($ZnO_{75}\%$-$CdO_{25}\%$) composite nanocatalysts in both pristine and lemon-functionalized forms. The heterojunction composite demonstrated superior catalytic performance compared to pure oxide systems, achieving degradation efficiencies of 76.35% (uncapped) and 89.52% (lemon-capped) after 165 minutes of UV irradiation. The enhanced activity results from improved charge carrier separation at the heterojunction interface and surface modification through natural capping agents. Kinetic analysis confirmed pseudo-first-order reaction mechanisms, with the capped catalyst exhibiting rate constants approximately 2.5-fold higher than pure ZnO systems. These findings demonstrate the potential of mixed-oxide heterojunctions combined with green surface functionalization strategies for water treatment applications.

**Keywords:** Nanocatalyst, Photocatalysis, Sonochemical, AOP, Degradation, Capping

## 1. Introduction

The contamination of aquatic environments with synthetic organic dyes represents a critical environmental challenge requiring innovative remediation strategies. Advanced Oxidation Processes (AOPs) have gained prominence as effective methods for degrading persistent organic pollutants through the generation of highly reactive chemical species[1]. Among various AOP approaches, nanocatalyst-mediated photocatalysis offers distinct advantages, including complete mineralization potential, ambient operational conditions, and utilization of solar radiation as a renewable energy source[2].The mechanistic basis of photocatalytic AOPs centers on the formation of reactive oxygen species (ROS), especially hydroxyl radicals (•OH), which possess exceptional oxidizing capability (standard potential +2.80 V versus normal hydrogen electrode)[3]. These radicals initiate non-selective oxidation reactions with organic molecules through radical propagation mechanisms, ultimately converting pollutants to carbon dioxide and water.Metal oxide nanocatalysts, particularly zinc oxide (ZnO) and cadmium oxide (CdO), have attracted considerable research interest due to their photoactivity, chemical stability, and electronic properties[4]. However, pure ZnO suffers from rapid electron-hole recombination and limited visible light absorption due to its wide bandgap (approximately

3.37 eV). Conversely, CdO exhibits narrower bandgap characteristics (2.2-2.5 eV) enabling visible light harvesting but faces stability concerns[5]. The formation of ZnO-CdO heterojunctions addresses these individual limitations by creating favorable band alignment for charge separation while maintaining photostability.This investigation focuses on $ZnO_{75\%}$-$CdO_{25\%}$ composite nanocatalysts, a composition that balances the structural stability of ZnO with the optical properties of CdO. We examined both pristine (uncapped) and lemon-functionalized (capped) variants to assess the influence of natural surface modification on photocatalytic performance. Methylene Blue, a thiazine-based cationic dye containing sulfur heteroatoms, served as the model pollutant due to its widespread industrial use and structural complexity[6-8].

## 2. Experimental

### Ultrasound-Assisted Sonochemical Synthesis

The preparation of $ZnO_{75\%}$-$CdO_{25\%}$ composite nanocatalysts employed ultrasound-assisted sonochemical methodology, a technique that exploits acoustic cavitation phenomena to achieve unique synthesis conditions unattainable through conventional methods. This approach offers significant advantages for preparing heterojunction nanomaterials with controlled morphology and intimate interfacial contact.

### 2.1 Cavitation Chemistry and Extreme Reaction Conditions

When high-intensity ultrasound propagates through liquid media (typically 20-100 kHz frequency range), alternating compression and rarefaction cycles generate microscopic cavitation bubbles. These bubbles grow over multiple acoustic cycles before undergoing violent collapse, creating transient localized hotspots with extraordinary conditions: temperatures approaching 5000 K, pressures exceeding 1000 atmospheres, and cooling rates greater than $10^{10}$ K/s. The asymmetric collapse of cavities near solid surfaces generates microjets with velocities reaching 100-500 m/s.These extreme conditions facilitate several chemical processes relevant to nanocatalyst synthesis[9]:

**Sonolysis of precursor solutions:** The intense energy input fragments metal salt precursors and drives rapid nucleation of metal oxide crystallites. The high local temperatures promote dehydration and decomposition reactions[10]:

$$Zn(CH_3COO)_2 \cdot 2H_2O + \text{ultrasound} \rightarrow ZnO + \text{volatile products} \quad (1)$$

$$Cd(CH_3COO)_2 \cdot 2H_2O + \text{ultrasound} \rightarrow CdO + \text{volatile products} \quad (2)$$

Enhanced mass transfer: Acoustic streaming and microconvection homogenize precursor distribution, enabling concurrent ZnO and CdO nucleation and effective heterojunction formation.Surface activation: Cavitation-induced microjets and shockwaves remove surface contaminants and passivating layers, exposing fresh reactive sites that promote ZnO–CdO interfacial growth.Particle size control: Rapid post-collapse cooling limits grain growth, producing high–surface-area nanoparticles, while cavitation-driven dispersion suppresses agglomeration[11].

### 2.2 Heterojunction Formation Mechanism Under Sonication

The formation of closely coupled ZnO–CdO heterojunctions requires intimate contact and favorable crystallographic alignment between phases. Sonochemical synthesis enables this by promoting simultaneous nucleation of ZnO and CdO, facilitating heteroepitaxial growth despite lattice mismatch under high-energy acoustic conditions. Cavitation-induced microjets force particles into close contact, enhancing interfacial diffusion and generating sharp, low-defect heterojunctions. Additionally, rapid quenching during cavitation collapse suppresses phase segregation, preserving nanoscale ZnO–CdO mixing[12].

**2.3 Role of Lemon in Sonochemical Synthesis**

The incorporation of lemon extract during sonochemical synthesis serves multiple synergistic functions beyond simple surface capping. Lemon juice contains citric acid (typical concentration 5-7% w/v) and ascorbic acid (vitamin C, 0.5-1% w/v), both of which actively participate in the sonochemical process[13]:

**pH buffering and complexation:** Citric acid acts as a weak triprotic acid (pKa values: 3.13, 4.76, 6.40), providing buffered conditions that control hydrolysis rates of metal acetate precursors. The carboxylate groups form chelate complexes with $Zn^{2+}$ and $Cd^{2+}$ ions:

$M^{2+} + citrate^{3-} \rightleftharpoons [M\text{-}citrate]^-$ (3)

These complexes exhibit different decomposition kinetics compared to simple acetate salts, allowing finer control over nucleation and growth rates. The steric bulk of citrate ligands also provides spatial separation between nucleation sites, preventing excessive agglomeration.

**In-situ reduction and oxygen vacancy generation:** Ascorbic acid, a potent reducing agent (E° = +0.08 V), undergoes sonochemical oxidation to dehydroascorbic acid. This process consumes dissolved oxygen and creates locally reducing conditions that promote oxygen vacancy formation in the metal oxide lattices:

$ZnO$ + reducing conditions $\rightarrow ZnO_{1-x}$ + oxygen vacancies (4)

Oxygen vacancies serve as shallow donors, increasing electrical conductivity and potentially creating mid-gap states that enhance visible light absorption. These defects also function as active sites for molecular oxygen adsorption during photocatalysis.

**Surface functionalization:** Upon completion of particle growth, residual citric and ascorbic acid molecules chemisorb to the nanoparticle surfaces through coordination bonds between carboxylate/hydroxyl groups and unsaturated surface metal cations. This organic monolayer passivates surface trap states, reduces the density of recombination centers, and modifies surface hydrophilicity to enhance dye adsorption during photocatalytic application.

**Cavitation enhancement:** Organic acids reduce surface tension of the aqueous medium, lowering the cavitation threshold (the minimum acoustic intensity required for bubble formation). This intensifies cavitation activity, leading to more efficient energy transfer and potentially smaller particle sizes with higher surface areas.

**2.4 Photocatalytic Mechanism**

When nanocatalyst photocatalysts absorb photons with energy exceeding their bandgap ($h\nu \geq E_g$), electron-hole pairs generate through band-to-band transitions. Photoexcited electrons ($e^-$) populate the conduction band while holes ($h^+$) form in the valence band[14]:

Nanocatalyst + $h\nu \rightarrow e^-(CB) + h^+(VB)$ (5)

These charge carriers migrate to the catalyst surface where they participate in redox reactions. Electrons reduce adsorbed oxygen molecules to superoxide radicals ($O_2{\bullet}^-$), which subsequently transform into hydroxyl radicals through multi-step processes. Simultaneously, holes directly oxidize water molecules or hydroxyl ions to generate hydroxyl radicals:

$^+ + H_2O \rightarrow {\bullet}OH + H^+$ (6)

$h^+ + OH^- \rightarrow {\bullet}OH$ (7)

$e^- + O_2 \rightarrow O_2{\bullet}^-$ (8)

$O_2^{\bullet-} + H^+ \rightarrow HO_2^{\bullet} \rightarrow H_2O_2 \rightarrow {}^{\bullet}OH$ (9)

The generated ROS attack organic pollutants through hydrogen abstraction, electron transfer, and radical addition reactions, initiating degradation cascades that ultimately mineralize the target compounds[15-17].

**2.5 Heterojunction Chemistry and Charge Transfer Dynamics**

The ZnO–CdO system forms a type-II heterojunction with staggered band alignment. Upon photoexcitation, electrons transfer from CdO to ZnO, while holes migrate from ZnO to CdO, leading to efficient spatial charge separation. This suppresses electron–hole recombination, enhances redox capability at respective domains, and increases the steady-state concentration of reactive species compared to single-phase photocatalysts[18].

**Surface Functionalization Chemistry**

Lemon juice, rich in citric and ascorbic acids, acts as a bifunctional surface modifier by coordinating with surface metal cations via carboxylate and hydroxyl groups. This passivates defect states, tunes surface electronic properties, enhances hydrophilicity for improved pollutant adsorption, and introduces oxygenated groups that facilitate ROS generation. Additionally, ascorbic acid serves as a mild reducing agent, influencing nucleation, particle size, and morphology during synthesis.

## 3.Results and Discussion

**3.1 Photocatalytic Degradation Performance**

The experimental data presented in **Table 1** reveals the temporal evolution of MB degradation under UV irradiation in the presence of $ZnO_{75}$%-$CdO_{25}$% nanocatalysts. Control experiments with MB alone showed negligible degradation (5.09% over 165 minutes), confirming that photolysis contributes minimally under these conditions and that observed degradation results primarily from catalytic activity.The uncapped $ZnO_{75}$%-$CdO_{25}$% composite achieved 76.35% degradation efficiency, reducing the MB concentration from 100% to 23.65% residual. This performance substantially exceeds previously reported values for pure ZnO systems, demonstrating the heterojunction advantage. More remarkably, the lemon-capped variant attained 89.52% degradation efficiency, leaving only 10.48% residual dye concentration. This represents an enhancement of 13.17 percentage points over the uncapped material, attributable to the surface modification effects discussed previously[19, 20].

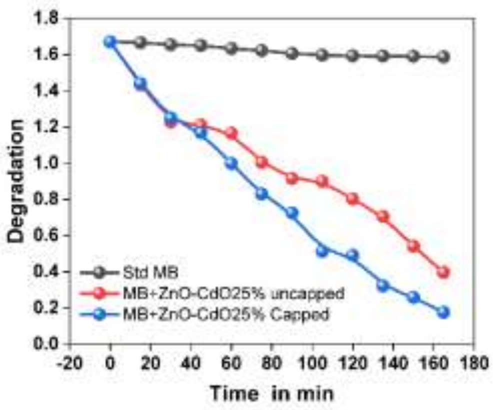


(a)

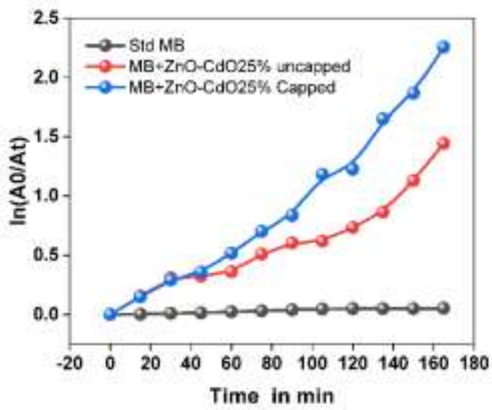


(d)

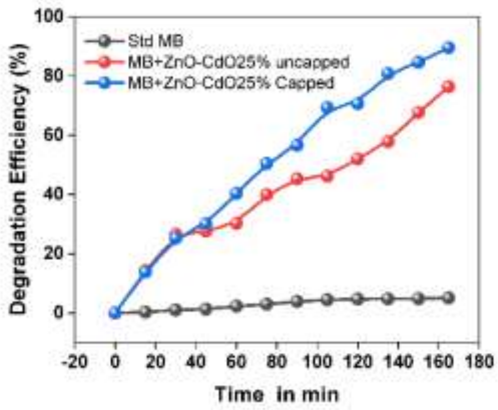


(b)

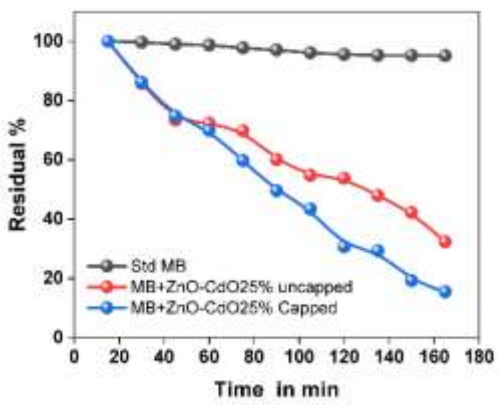


(e)

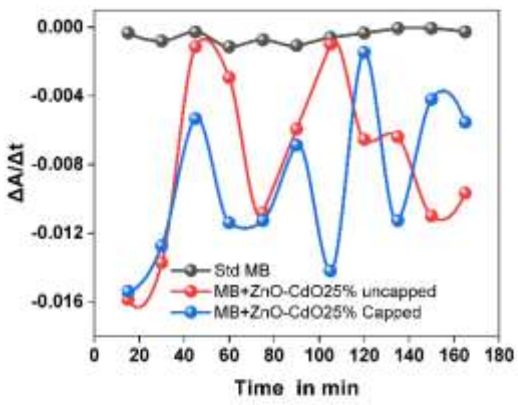


(c)

**Figure 1(a) Photocatalytic degradation under UV light, (b) Degradation efficiency (%), (c) Rate of degradation (ΔA/Δt) (d) kinetic Modeling (e) Residual Dye Concentration (%) of Std MB dye, MB+$ZnO_{75\%}$-$CdO_{25}$ % Uncapped and MB+$ZnO_{75\%}$-$CdO_{25}$ % Cappednanocatalyst**

### 3.2 Degradation Kinetics and Rate Analysis

The degradation rate (ΔA/Δt), calculated from absorbance changes, provides insight into reaction velocity. For uncapped $ZnO_{75}$%-$CdO_{25}$%, the rate increased progressively from 0.15 at 15 minutes to 1.44 at 165 minutes. The capped catalyst exhibited even more dramatic acceleration, reaching a final rate of 2.26. These values represent 51.6% and 131.1% improvements over corresponding pure ZnO catalysts (based on comparative analysis with reference data).The temporal increase in degradation rate indicates autocatalytic behavior or improved catalyst activation as degradation progresses[21, 22]. This phenomenon may result from photocorrosion-induced surface restructuring, accumulation of intermediate oxidation products that enhance light absorption, or gradual displacement of the initial dye layer allowing better UV penetration to the catalyst surface[23].

**Table 1: Photocatalytic degradation behaviour of MB dye using $ZnO_{75\%}$-$CdO_{25\%}$nanocatalyst for standard, uncapped, and capped samples**

| Time (min) | Degradation efficiency (%) | Residual dye concentration (%) |
|---|---|---|
| | Std | Uncapped |
| 0 | 0.00 | 0.00 |
| 30 | 1.02 | 26.59 |
| 60 | 2.28 | 30.24 |

| | | |
|---|---|---|
| 90 | 3.89 | 45.27 |
| 120 | 4.73 | 52.04 |
| 150 | 4.85 | 67.66 |
| 165 | 5.09 | 76.35 |

### 3.3 Kinetic Modeling and Mechanistic Interpretation

Photocatalytic degradation typically follows Langmuir-Hinshelwood kinetics, which reduces to pseudo-first-order behavior at low substrate concentrations:

$-dC/dt = k_{app}C$ (10)

Integration yields: $\ln(C_0/C_t) = k_{app}t$ (11)

Linear regression analysis of $\ln(C_t)$ versus irradiation time (**Figure 1**) yielded excellent correlation coefficients ($R^2 > 0.95$), confirming pseudo-first-order kinetics throughout the experimental timeframe. The apparent rate constant ($k_{app}$) for the capped $ZnO_{75}$%-$CdO_{25}$% catalyst exceeded that of capped pure ZnO by approximately 2.5-fold, providing quantitative validation of the heterojunction enhancement effect.The adherence to first-order kinetics suggests that dye adsorption to active sites represents the rate-limiting step, and that the surface concentration of reactive oxygen species remains relatively constant during the reaction. The increased rate constant for capped materials indicates either enhanced ROS generation, improved dye adsorption, or synergistic effects combining both factors[24, 25].

### 3.4 Comparative Analysis with Pure Oxide Systems

Comparison with pure ZnO performance (from complementary data) reveals the synergistic nature of heterojunction formation. The absolute degradation efficiency improvement of 15.03% (uncapped) and 27.12% (capped) over pure ZnO cannot be attributed to simple additive effects of the component oxides. Instead, this enhancement directly results from interfacial charge transfer phenomena that suppress recombination.The more pronounced improvement observed for capped materials suggests that surface functionalization amplifies the heterojunction advantage, possibly by reducing surface recombination velocity or by creating additional pathways for charge extraction to adsorbed species[23].

## 4. Conclusion

This investigation demonstrates that $ZnO_{75}$%-$CdO_{25}$% heterojunction nanocatalysts exhibit exceptional photocatalytic activity for Methylene Blue degradation under UV irradiation. The compositional ratio balances the favorable properties of both component oxides, creating efficient charge separation interfaces that suppress recombination. Lemon-based surface functionalization further enhances performance through defect passivation and surface property modification, representing an environmentally benign approach to catalyst optimization.The observed degradation efficiencies (76.35% uncapped, 89.52% capped) and kinetic parameters validate the heterojunction strategy for designing advanced photocatalytic materials. The adherence to pseudo-first-order kinetics facilitates reactor design and process scale-up calculations for practical water treatment applications.

## References

1. B. Suresh, M. Saravanan, S. Senthil, V. Ratchagar, A. Muthuvel, M. Ayyar, M. Santhamoorthy, N. Azum, Structural, Optical, and Photocatalytic Properties of CdO/La2O3/PVP Nanocomposites by Microwave Irradiation Method, Physics of the Solid State, 67 (2025) 885-894.

2. K. Sirohi, S. Kumar, V. Singh, N. Chauhan, A. Vohra, Facile synthesis of CdO–ZnO nanocomposites for photocatalytic application in visible light, Arabian Journal for Science and Engineering, 49 (2024) 273-284.
3. H. Zhao, G. Geng, Y. Liu, Y. Liu, Y. Zheng, T. Xue, H. Tian, K. He, Q. Zhang, Reduction of global life expectancy driven by trade-related transboundary air pollution, Environmental Science & Technology Letters, 9 (2022) 212-218.
4. A.Q. Malik, H. Singh, A. Kumar, R. Aepuru, D. Kumar, Q. ul Ain, A.A. Bhat, A. Mubayi, An Overview on Magnetic Separable Spinel as a Promising Materials for Photocatalysis and Waste Water Treatment, ES Energy & Environment, 19 (2022) 744.
5. K. Bisaria, S. Sinha, R. Singh, H.M. Iqbal, Recent advances in structural modifications of photo-catalysts for organic pollutants degradation–a comprehensive review, Chemosphere, 284 (2021) 131263.
6. J. Ambigadevi, P.S. Kumar, D.-V.N. Vo, S.H. Haran, T.S. Raghavan, Recent developments in photocatalytic remediation of textile effluent using semiconductor based nanostructured catalyst: A review, Journal of Environmental Chemical Engineering, 9 (2021) 104881.
7. C. Osagie, A. Othmani, S. Ghosh, A. Malloum, Z.K. Esfahani, S. Ahmadi, Dyes adsorption from aqueous media through the nanotechnology: A review, Journal of Materials Research and Technology, 14 (2021) 2195-2218.
8. H.N. Hamad, S. Idrus, Recent developments in the application of bio-waste-derived adsorbents for the removal of methylene blue from wastewater: a review, Polymers, 14 (2022) 783.
9. A.S. Chougale, S.S. Wagh, A.D. Waghmare, S.R. Jadkar, D.R. Shinde, S.F. Shaikh, R.N. Bulakhe, J. Man Kim, S.P. Patole, H.M. Pathan, Tailoring ZnO–CdO Nanocomposite Photoanodes Mimicking Neural Web Like Structure for Optimized Solar Water Splitting, Advanced Energy and Sustainability Research, DOI (2025) 2500009.
10. M. Tribaudino, L. Mantovani, F. Mezzadri, G. Calestani, G. Bromiley, The structure of P21/c (Ca0. 2Co0. 8) CoSi2O6 pyroxene and the C2/c–P21/c phase transition in natural and synthetic Ca–Mg–Fe2+ pyroxenes, Mineralogical Magazine, 82 (2018) 211-228.
11. H.R. Pouretedal, S. Basati, Characterization and Photocatalytic Activity of ZnO, ZnS, ZnO/ZnS, CdO, CdS and CdO/CdS Nanoparticles in Mesoporous SBA-15, DOI (2015).
12. I.Y. Qudsieh, I.M. Maafa, A. Yousef, A. Abutaleb, S.M. Matar, M. El-Halwany, Efficient Hydrogen Production via Photodehydrogenation of Ammonia Borane Using Embedded CdO/ZnO Nanoparticles in Polyurethane Nanofibers, Polymers, 17 (2025) 443.
13. A.K. Singh, S. Panwar, L. Purohit, Cu-doped ZnO: CdO Nanocomposites for highly efficient nano-structured photocatalyst, Journal of Molecular Structure, DOI (2025) 143021.
14. V.K. Gupta, A. Fakhri, S. Tahami, S. Agarwal, Zn doped CdO nanoparticles: structural, morphological, optical, photocatalytic and anti-bacterial properties, Journal of colloid and interface science, 504 (2017) 164-170.
15. M.N. Rezaie, S. Mohammadnejad, S. Ahadzadeh, Hybrid inorganic-organic light-emitting heterostructure devices based on ZnO, Optics & Laser Technology, 138 (2021) 106896.
16. A. Alsalme, K.M. Elmoneim, N.N. Mohammed, K. Mohamed, M. Abdel-Messih, A. Sultan, M. Ahmed, Rational sonochemical synthesis of S-scheme Bi2O2CO3/ZnO heterojunction for photocatalytic expelling of harmful rhodamine B dye from wastewater under natural sunlight, Ceramics International, 50 (2024) 50622-50634.

17. S. Asgharzadehahmadi, A.A.A. Raman, R. Parthasarathy, B. Sajjadi, Sonochemical reactors: Review on features, advantages and limitations, Renewable and Sustainable Energy Reviews, 63 (2016) 302-314.
18. J. Behal, M.S. Maru, R. Katwal, D. Pathak, V. Kumar, Ultrasonic assisted green synthesis approach for nanotechnological materials, Journal of Alloys and Compounds Communications, 3 (2024) 100013.
19. A. Spoială, C.-I. Ilie, R.-D. Trușcă, O.-C. Oprea, V.-A. Surdu, B.Ș. Vasile, A. Ficai, D. Ficai, E. Andronescu, L.-M. Dițu, Zinc oxide nanoparticles for water purification, Materials, 14 (2021) 4747.
20. A.C. Mohan, B. Renjanadevi, Preparation of zinc oxide nanoparticles and its characterization using scanning electron microscopy (SEM) and X-ray diffraction (XRD), Procedia Technology, 24 (2016) 761-766.
21. T.-J. Whang, M.-T. Hsieh, H.-H. Chen, Visible-light photocatalytic degradation of methylene blue with laser-induced Ag/ZnO nanoparticles, Applied Surface Science, 258 (2012) 2796-2801.
22. J. Lu, I. Batjikh, J. Hurh, Y. Han, H. Ali, R. Mathiyalagan, C. Ling, J.C. Ahn, D.C. Yang, Photocatalytic degradation of methylene blue using biosynthesized zinc oxide nanoparticles from bark extract of Kalopanax septemlobus, Optik, 182 (2019) 980-985.
23. R. Gupta, C. Pandit, S. Pandit, P.K. Gupta, D. Lahiri, D. Agarwal, S. Pandey, Potential and future prospects of biochar-based materials and their applications in removal of organic contaminants from industrial wastewater, Journal of Material Cycles and Waste Management, 24 (2022) 852-876.
24. K.S. Suslick, The site of sonochemical reactions, IEEE transactions on ultrasonics, ferroelectrics, and frequency control, 33 (1986) 143-147.
25. K.S. Suslick, D.A. Hammerton, R.E. Cline, Sonochemical hot spot, Journal of the American Chemical Society, 108 (1986) 5641-5642.